The Hunting-style Deployment of Underwater Sensor Networks

NA XIA and YIN WANG, Hefei University of Technology, China
QIONG WU, HuaNeng Power International Inc. Anhui Wind Power Branch, China
CHENGUANG YUAN, China HuaNeng Group Co., Ltd. Anhui Branch, China
XINYI WEN and YUE WU, Hefei University of Technology, China
LONGYA LANG, Anhui JiYuan Software Co., Ltd., China

Underwater pollution incidents occur frequently, and obtaining accurate information about their exact location and real-time situation is helpful for promptly formulating plans to contain and mitigate the situation. Autonomously adjusting the position of sensors for optimal coverage and monitoring of regions of interest (e.g., oil spill zones, chemical contamination areas) in real time is a significant challenge. To this end, this article proposes a hunting-style underwater sensor deployment based on the level set method. This method uses a gateway-like role to calculate the boundary and other parameters of the interest region based on an energy function used for positioning sensors. Subsequently, the sensors use these parameters as the basis to complete their migration toward the boundary of the interest region. This sensor migration can gradually evolve into a hunting deployment for the interest region. This article also proposes two novel performance evaluation metrics–structural similarity and network energy balance–to evaluate the comprehensive performance of the proposed hunting-style deployment of underwater sensors. Extensive simulation experiments demonstrate the effectiveness of the proposed method.

CCS Concepts: • **Networks** → **Network architectures**; **Network algorithms;**

Additional Key Words and Phrases: Underwater sensor networks, hunting style, deployment, level set method, Structural Similarity

ACM Reference format:
Na Xia, Yin Wang, Qiong Wu, ChenGuang Yuan, Xinyi Wen, Yue Wu, and LongYa Lang. 2023. The Hunting-style Deployment of Underwater Sensor Networks. *ACM Trans. Sensor Netw.* 19, 4, Article 96 (July 2023), 22 pages.
https://doi.org/10.1145/3604556

This work was support in part by the National Natural Science Foundation of China under Grant 61971178 and Grant 61701161; in part by Science and Technology Major Project of Anhui Province under Grant 18030901015; in part by Demonstration of Comprehensive Application of Beidou in Anhui Province under Grant ZF2022-08-0020, and State Grid Co., Ltd. Headquarters Technology Project under Grant 5500-202140127A.
Authors' addresses: N. Xia, Y. Wang (corresponding author), X. Wen, and Y. Wu, Hefei University of Technology, Hefei, China, 230009; emails: xiananawo@hfut.edu.cn, wangyin950203@gmail.com, 2018110984@mail.hfut.edu.cn, WuYue525hhh@163.com; Q. Wu, HuaNeng Power International Inc. Anhui Wind Power Branch, Hefei, China, 230031; email: 421344405@qq.com; C. Yuan, China HuaNeng Group Co., Ltd. Anhui Branch, Hefei, AnHui, China, 230022; email: 44899153@qq.com; L. Lang, Anhui JiYuan Software Co., Ltd., Hefei, AnHui, China, 230088; email: langlongya@sgitg.sgcc.com.cn.

1550-4859/2023/07-ART96 $15.00
https://doi.org/10.1145/3604556

1 INTRODUCTION

The ocean covers most of the Earth's surface and is abundant in species and resources while also serving as a means for global trade. This makes the development of human society highly dependent on the ocean [27, 34, 38]. However, with the development and utilization of the ocean by humankind, various kinds of marine pollution issues have arisen, including oil diffusion areas formed by oil spills on the water's surface and polluted areas formed by pollutant discharge in water bodies. Therefore, there is an urgent need to carry out research on monitoring and tracking polluted marine areas.

As a new method to explore and use the ocean, **underwater sensor networks (UWSNs)** have been widely applied to multiple fields such as ocean information collection, geological disaster prevention, resource exploration, and military monitoring, playing an important role in detection and monitoring of underwater areas that are not easily accessible to people; therefore, it has become a hotspot in the field of sensor network research [15, 21, 32]. In recent years, the research direction regarding UWSNs has mainly focused on underwater wireless communication technology [22, 45], node deployment [19, 31], network system design [10, 13], data collection [39, 44], protocol design [7, 48], and location tracking [36, 43]. Among these, the arrangement of sensor nodes is a fundamental issue in the application of UWSNs. It provides support for network topology, target monitoring, data routing, and other application fields. In marine pollution monitoring, powerful computing capabilities can help nodes monitor, analyze, and respond to marine pollution events in real time, providing high-quality data support. The use of underwater wireless communication technology enables the establishment of reliable sensor networks, ensuring accurate data transmission and reception. Therefore, powerful computing capabilities and underwater wireless communication technology play an important role in marine pollution monitoring. Reasonable node deployment can integrate **mobile edge computing (MEC)** [3, 40] and underwater communication technology, improve service quality and efficiency, and unleash the tremendous potential of sensor networks in marine pollution monitoring applications.

However, existing underwater node deployment schemes have not fully considered the shape of the monitoring targets or achieved real-time tracking of the region of interest. They fail to capture dynamic changes occurring in the regions of interest, such as the spread of pollutants such as oil or nuclear waste, algal blooms, and so on. Therefore, it is necessary to research a self-organizing deployment mechanism for nodes in the region of interest. With this motivation, we propose a sensor node deployment method based on the **level set method (LSM)** for tracking the morphological edges of the region of interest in conjunction with emerging underwater mobile MEC technology. Sensor nodes calculate the movement parameters according to the topological structure of the region of interest and then move solitarily. Nodes move in real time according to the topological structure of the region of interest, ensuring continuous tracking and monitoring. The main contributions of the article are as follows:

(1) We propose a hunting-style deployment model using a multilayered distribution of mobile nodes to monitor changes in the region of interest in real time, particularly for tracking underwater pollution.
(2) We use LSM to track the region of interest. This method uses a gateway-like role to calculate the boundary and other parameters of the interest region based on an energy function used for positioning sensors. Subsequently, the sensors use these parameters as the basis to complete their migration toward the boundary of the interest region.
(3) We propose two novel performance evaluation metrics—structural similarity index and network energy balance—to evaluate the comprehensive performance of our proposed

hunting-style deployment of underwater sensors. Extensive simulation experiments demonstrate the effectiveness of the proposed method.

The rest of the article is arranged as follows: Section 2 briefly analyzes and summarizes related work on node deployment in UWSNs. Section 3 presents the network model and corresponding concepts. Section 4 describes the **sensor deployment method based on the level set method (SD-LSM)** and puts forward two performance evaluation indicators for node deployment. In Section 5, we design our sets of simulation experiments, which evaluate our proposed method's effectiveness. Conclusions are drawn in Section 6.

2 BACKGROUND AND RELATED WORK

In land sensor networks, there are abundant theoretical achievements and application cases regarding the deployment of sensor nodes. However, due to the great disparity between land and underwater environments, related findings cannot be directly applied to UWSNs. Given the main purpose of this work, we discuss related work regarding the following two aspects: static node deployment for underwater monitoring and mobile node deployment for underwater target tracking.

2.1 Static Node Deployment for Underwater Monitoring

2.1.1 Area Coverage Node Deployment. Wang et al. [41] studied an underwater sensor node depth-determination method. This method uses a breadth-first or depth-first search algorithm to check network connectivity. In addition, the Voronoi diagram is used to detect coverage loopholes of underwater nodes and apply the K-means clustering algorithm to adjust the depth of remaining nodes on the water surface to repair coverage loopholes. Jin et al. [17] also studied a node optimization arrangement mechanism based on depth adjustment. By adjusting the depth of the node, the method reduces repeated coverage areas between the sensor node and neighboring nodes and, furthermore, optimizes the coverage area of the sensor network. Cobanlar et al. [50] create an optimization framework to model the effects of the k value on UWSN lifetime, which is utilized to characterize the tradeoff between k-connectivity and network lifetime. Su et al. [35] proposed a Voronoi-based optimal depth adjustment deployment scheme, wherein gateways collect coordinates of sensor nodes to build Voronoi diagrams. Certain sensor nodes are selected to remain on the water surface based on this diagram, called leader nodes. The remaining nodes need to be sunk to different depths to reduce coverage overlap between nodes.

2.1.2 Event Coverage Node Deployment. Jiang et al. [16] proposed a UWSNs redeployment algorithm based on wolves. The algorithm mimics the wolf's predator mechanism and combines crowding control to ensure event coverage while avoiding getting trapped in local optimality. To some extent, this algorithm solves the problem concerning node redeployment in UWSNs. Arivudainambiet et al. [2] adopted the cuckoo search algorithm to find the optimal location so nodes can achieve single coverage of specific underwater targets. To address the problems of node deployment schemes that lack consideration of network connectivity and high deployment costs, an improved moth flame optimization node deployment algorithm based on fuzzy operators is proposed [42]. The algorithm is capable of improving network coverage with a limited number of nodes while ensuring full connectivity.

2.1.3 Specific Node Deployment. Zhang et al. [46] designed a 2D water gateway optimization deployment algorithm based on improved cuckoo search, using the advantage of the improved algorithm to solve the optimal layout of the surface gateway, which not only equalizes the number of underwater nodes covered by each surface gateway but also minimizes the signal propagation

delay. Al-Saltiet et al. [1] designed a method to determine the surface sink node of UWSNs, which utilizes the approach of dividing around a central point. In this method, a fixed number of nodes are selected as sink nodes among the surface candidates by iterative calculation to minimize the total number of hops of data transmission between underwater sensor nodes and sink nodes. Liu et al. [25] studied adding relay nodes to a deployed UWSN to compensate for the shortcomings of the original network topology. Under the guidance of the heuristic algorithm, the node sinks to the appropriate position to serve as the communication relay between distant nodes. This method helps achieve the goal of optimizing the network and extending its life. Some scholars have further studied the problem of using relay nodes to repair network isolation caused by underwater node failure [24]. Fermat point selection algorithm has been used to optimize the deployment scheme of relay nodes. Kahriman et al. [18] present an SG placement optimization model that maximizes sensor coverage. The optimal location is compared with the benchmark location computed by averaging the location of underwater sensors. To monitor river temperature at a microhabitat scale, Burman et al. [5] deployed and optimized a wireless sensor network and proposed a node software architecture based on event-driven proto-threads. The architecture was explicitly designed to minimize power consumption to ensure long-term operation of the nodes. In addition, they designed a methodology to correct the data timestamp with incremental identifiers.

2.2 Mobile Node Deployment for Underwater Target Tracking

At present, significant progress has been made in research on using **autonomous underwater vehicles (AUVs)** for underwater target tracking. Ge et al. [9] proposed an algorithm for multi-AUV hunting of target event points in surface water environments. This method models the information of the surface water environment using artificial potential field theory and introduces the dispersion degree, homodromous degree, and district-difference degree into the potential field function to address the target hunting problem. Guo et al. [11] developed a path-planning model for simultaneously optimizing the direction and speed of **unmanned surface vehicles (USVs)** to search for submarines. By introducing three control factors to adaptively control the direction and amplitude of mutation, an improved genetic algorithm maximized the cumulative detection probability. In Reference [49], Zhu et al. used a **biologically inspired neural network (BINN)** map to allocate target-tracking tasks to AUVs. After calculating the activity values of all AUVs in the BINN graph of each target, the AUV with the highest activity value is designated the winning AUV for that target, and the path planning is performed according to the BINN strategy. Han et al. [12] devised a unified framework to consistently address the problem of task allocation in both nonemergency and emergency cases. They reinforced the self-organizing map method with three strategies'regional learning rate, self-configuring neuron strategy, and workload balancing mechanism to ensure the effectiveness and adaptability of unified task allocation.

To detect oil spills from container ships in coastal areas, Kumar et al. [20] used AUVs for search operations and proposed a hybrid evolutionary optimization algorithm called whale cuckoo search optimization algorithm to determine the optimal path. This algorithm effectively reduces the overall search delay and minimizes energy consumption of AUVs. Lin et al. [23] utilized the paradigm of software-defined networking to enhance the flexibility of underwater wireless networks based on AUV swarms. Taking advantage of the centralized management characteristic of software-defined networking, they introduced the concept of AUV swarms and proposed a unified control model based on artificial potential field theory to perform precise underwater path-planning tasks. To efficiently manage the network, Qi et al. [29] developed a control model based on artificial potential field and network topology theory. Building on the proposed network architecture, they also presented a proactive alarming-enabled path-planning scheme that accounts for all potential categories in obstacle-avoidance scenarios.

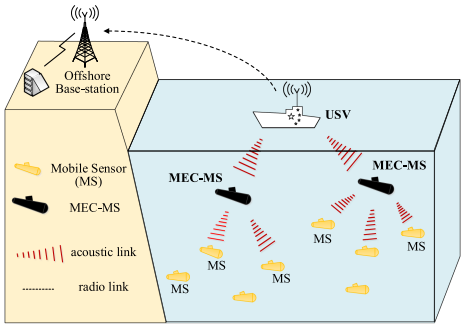

Fig. 1. Architecture of underwater acoustic sensor networks.

In the context of static node deployment for underwater monitoring, the primary goal is to ensure full coverage of the monitoring area or specific event points. However, this approach falls short in its ability to capture the regions of interest (2D or 3D regions) dynamically and in real time. In the context of underwater target tracking based on dynamic nodes, existing methods primarily focus on assigning task points to AUVs or planning the shortest paths to cover all oil spill areas without real-time tracking of regions of interest. This approach fails to capture dynamic changes occurring in the interest regions, such as the spread of pollutants such as oil or nuclear waste, algal blooms, and so on. Different from existing works, we propose a method for hunting deployment of underwater sensors based on LSM, employing mobile nodes to track regions of interest in real -time. This method uses the morphological characteristics of the interest region to drive the sensor nodes to migrate to boundaries in a self-organized way and move autonomously with the expansion of the interest region to acquire and track the event, which enables hunting-style node deployment.

3 PRELIMINARIES

3.1 Network Architecture

We consider a multilayer underwater sensor network structure, as shown in Figure 1. The network consists of a USV deployed on the surface and mobile sensors deployed underwater, such as AUVs and underwater robotic vehicles. Mobile sensors deployed underwater are subdivided into two categories: **mobile sensor (MS)** and **mobile sensor control terminals (MEC-MS)**. For the sake of convenience, in this article, mobile sensor (MS) is also referred to as sensor node or node. These sensor nodes are equipped with advanced underwater sensing equipment and distributed in specific underwater areas to perform searches or monitoring. They are responsible for collecting and storing information about the surrounding environment, such as concentration, salinity, water temperature, and so on. Sensor nodes transmit monitored or collected data to MEC-MSs regularly to inform decisions.

MEC-MSs manage monitoring tasks by sending or receiving query messages to and from sensor nodes through a dedicated acoustic channel. MEC-MSs need to keep abreast of the network topology and positioning and trajectory tracking of sensor nodes in the designated domain. They are also responsible for managing the cruise direction, speed, and cooperative search of sensor nodes. An MEC-MS controls a sensor node cluster, and the number of sensor nodes depends on the efficiency requirements of the MEC-MS. Communication units are determined based on the computing power of the MEC-MS and the distribution range of sensor nodes. Therefore, the computing power required by MEC-MSs is much greater than that of sensor nodes. We introduce mobile edge-computing technology and deploy a lightweight edge-computing station on each MEC-MS device

to reduce the computing pressure and transmission delay of surface USVs. As a supercomputing unit, a USV deployed on the water surface further analyzes the information collected by multiple MEC-MSs to maintain the overall network topology structure and provide synchronization control information for the collaborative search of multiple sensor nodes. In addition, USVs are capable of connecting with an offshore base station via wireless communication technologies (e.g., radio or light waves), acting as MEC-MSs between sensor nodes and ground data centers.

We assume that there are d MEC-MSs and n sensor nodes in the UWSN. Let the set of MEC-MS be $G = \{g_1, g_2, \ldots, g_d\}$. All MEC-MS in the same network have the same wireless underwater acoustic communication and computational capability, and their communication distance is denoted as r^g. Let the set of sensor nodes be denoted as $S = \{s_1, s_2, \ldots, s_n\}$, and each sensor node $s_k (1 \leq k \leq n)$ has the ability to sense, communicate, and move. Denote the attribute vector of s_k as $\mathbf{B}_k =< r_k, l_k, \mathbf{p}_k, c_k >$, where $r_k \geq 0$, $l_k \geq 0$, and $\mathbf{p}_k$ describe the communication radius, maximal moving range, and the current position of s_k, respectively, and c_k is the concentration information sensed by s_k. All sensor nodes have the same attributes except for position and concentration in a homogeneous network, namely, $r_k = r^c$, $l_k = l (1 \leq k \leq n)$.

We judge whether there is pollution based on the molar value of the pollutant. As proposed in Reference [30], we model the concentration of pollutant chemicals in the water (that is, the molar value) as a function:

$$C(x,t) = \frac{M}{2 \cdot A\sqrt{\pi \cdot D_L \cdot t}} \cdot \exp[\frac{-(x - U \cdot t)^2}{4 \cdot D_L \cdot t}], \tag{1}$$

where x is the distance in the downstream direction expressed in meters (m), t is the duration between the spill and the monitoring at point x expressed in seconds (s), M is the mass of the contaminant expressed in kilograms, A is the cross-sectional area of the river expressed in m^2, D_L and U are longitudinal dispersion and advective velocity, respectively.

Definition 3.1 (Regional Computing Unit).

After the sensor node senses the interest region, the node sends the sensed information to the nearest MEC-MS. The MEC-MS then organizes the nodes in its communication range to form a computing unit, which is called a regional computing unit.

Upon observation, the hurdle in the self-organization of hunting underwater sensor nodes is to form multiple area calculation units in the monitoring area. In each area calculation unit, the MEC-MS calculates the interest region edge curve according to the sensor node's position information and perception information. Based on the calculated edge curve, the sensor node autonomously adjusts the deployment position so the nodes cover the edges of the interest region to realize the hunting-style node deployment.

3.2 Information Exchange Model

To achieve accurate tracking of underwater pollution, MEC-MS must obtain information of all sensor nodes in the designated area in a timely manner. We introduce two beacon messages based on the acoustic communication model, with TDMA protocol used in the MAC layer.

Report message (ReportMG). The report message is used by the sensor node to request positioning from the MEC-MS or by the MEC-MS to request positioning from the USA. After MEC-MS or USA receives the Report_request, MEC-MS or USA performs the positioning phase for the requested sensor node and returns the positioning estimation result to the requested sensor node through Report_reply.

Broadcast message (BroadcastMG). Sensor node sends its location and perceived concentration information to MEC-MS through Broadcast_request, which is represented by a triple (ID_k, $\mathbf{p}_k$, c_k). ID_k is the ID number of the sensor node. $\mathbf{p}_k$ is the location information of the MS, and c_k

is the perceived threshold density information. MEC-MS sends the boundary information of the polluted area and the concentration threshold information to sensor node via a Broadcast_reply, which is represented by a triple (ID_g, C_g, c_t). ID_g is the ID number of MEC-MS. C_g is the computed boundary curve of the polluted area, and c_t is the threshold information of the concentration perceived by sensor node.

3.3 Level Set Theory

LSM was first proposed by the famous American applied mathematician Osher [28] as a numerical method for interface tracking and shape modeling [4, 14, 37]. LSM maps the evolution calculation process of curve or surface to the Cartesian grid to avoid the process of parameterizing curve and surface. When the target shape is split or merged, the method can still effectively track the edge of the target shape. These characteristics make LSM widely used in many disciplines such as image processing, computational geometry, and optimization.

The basic idea of LSM is to transform the motion evolution of the m-dimensional curve into the m+1-dimensional function projection and implicitly solve the higher-dimensional function to accurately describe the topological structure of the low-dimensional curve plane. The implicit expression of the 2D plane curve C: $y = f(x)$, given as:

$$C = \{(x, y) \mid \varphi(x, y) = c\}, \tag{2}$$

where φ is the level set function and c is a constant. Curve C is the set of points that satisfy $\varphi(x, y) = c$ and is called a level set of level set function. Specifically, when $c = 0$, curve C is called the zero level set of the level set function.

Assuming that φ takes a positive value inside the curve and a negative value outside the curve, the unit normal vector of the level set can be expressed as:

$$\vec{n} = \frac{\nabla\varphi}{|\nabla\varphi|}, \tag{3}$$

where ∇ is the gradient operator.

In the process of topological optimization design based on LSM, the evolution of the curve can be regarded as the evolution of the level set function over time as:

$$C(t) = \{(x, y) \mid \varphi(x, y, t) = 0\}. \tag{4}$$

The derivative of Equation (4) with respect to time t is:

$$\frac{d\varphi}{dt} = \frac{\partial\varphi}{\partial t} + \nabla\varphi \cdot \frac{\partial(x, y)}{\partial t} = 0. \tag{5}$$

Because the evolutionary motion of curve C is not affected by the tangential component perpendicular to the gradient $\nabla\varphi$:

$$\frac{\partial(x, y)}{\partial t} = v \cdot \vec{n}, \tag{6}$$

where v is the velocity component of the curve in the normal direction, and $\vec{n}$ is the unit normal vector.

By substituting Equations (3) and (6) into Equation (5), we can obtain:

$$\frac{\partial\varphi}{\partial t} = v|\nabla\varphi|. \tag{7}$$

Equation (7) is the classic level set equation, also known as the Hamilton-Jacobi equation. It can be seen that the evolution process of LSM is the process of solving partial differential equations with

time. Equation (7) is an equation that evolves a continuous boundary. For numerical calculation, the level set equation needs to be discretized as:

$$\frac{\varphi_{ij}^{n+1} - \varphi_{ij}^{n}}{\Delta t} = \upsilon_{ij}^{n} | \nabla_{ij} \varphi_{ij}^{n} |. \tag{8}$$

Equation (8) can be solved by the finite difference method. Setting the edge of the interest region as the target curve, the process of nodes tending to the edge of the interest region is equivalent to the process of level set evolution tending to be stable. In this manner, the hunting-style deployment problem becomes an image segmentation problem that LSM can effectively address.

4 DEPLOYMENT METHOD OF SURROUNDING HUNTING UNDERWATER SENSOR NODES

4.1 2D Underwater Space Sensor Node Deployment

Multiple regions are set up within a monitoring area, and in each regional computing unit, USV calculates the edge curve of the region of interest based on the positions of sensor nodes and perceptual information. According to the calculated edge curve, the deployment position adjusts autonomously so the nodes cover the edge of the interest region to realize the surrounding node arrangement.

Based on the reliable theory described in Section 3.3, this research proposes a method of hunting deployment of underwater sensors based on LSM. SD-LSM is a adaptive node deployment method that consists of the following steps:

(1) Nodes transmit the collected pollution concentration and position information to the USV.
(2) The USV calculates the edge curve of the region of interest based on the information collected from the nodes.
(3) Nodes receive the edge curve sent by the USV and, based on the movement strategy, adjust their positions to move toward the edge curve.
(4) These steps repeat until the nodes reach the boundary of the region of interest.

4.1.1 Edge Curve Calculation. Level set theory is a classic digital image processing method and has a wide range of applications, including image detection, target recognition and tracking, image analysis, and more. Based on local target information, the regional LSM calculates the kinetic parameters to prompt the evolution curve to approach the target contour. Therefore, the regional method shows strong robustness against local dynamics and can suppress the influence of weak edges and environmental noise on the evolution process.

This research draws on the regional level set model called the Chan-Vese model [6] and uses the concentration information sensed by the nodes as energy to construct an energy function. The level set function corresponding to the minimum functional energy is solved through iteration. At this moment, the zero level set is the edge of the interest region.

The initial evolution curve must be set at the beginning of the model construction. To simplify the calculation complexity, a straight line parallel to the x-axis is selected as the initial curve. The level set function at time zero needs to be initialized before evolution begins, as:

$$\varphi(x, y, t = 0) = sign(x, y, C(t = 0)) \cdot dist(x, y, C(t = 0)). \tag{9}$$

This equation can be written as φ_o. $sign(x, y, C(t = 0))$ is a symbolic function. If the node is above the initial curve, then $sign(x, y, C(t = 0)) = +1$; otherwise, $sign(x, y, C(t = 0)) = -1$. $dist(x, y, C(t = 0))$ is the shortest Euclidean distance from the point (x, y) to the initial curve $C(t = 0)$. This initial function is also called the symbolic distance function. The calculation formula

of the energy functional is defined as:

$$E(c_m, c_n, C) = \mu \cdot \text{Length}(C) + \lambda \sum_{U_i} |c_k - c_i| + \lambda \sum_{U_o} |c_k - c_o|. \tag{10}$$

The first term in this equation is used to regulate the sensor nodes and is referred to as the regularization term. The second and third items are used to attract the sensor node to the target profile and are referred to as fidelity items. Here, c_k is the concentration information sensed by the sensor node, μ and λ are constant terms with a value of one, c_i is the mean value of the sensor node's perceived concentration inside the curve, and c_o is the mean value of the sensor node's perceived concentration outside the curve. U_i is the set of sensor nodes inside the curve, and U_o is the set of sensor nodes outside the curve.

Using the level set function $\varphi(x, y)$ instead of the evolution curve C, the energy functional is rewritten as follows:

$$E(c_i, c_o, C) = \mu \int_{\omega} \delta_\varepsilon(\varphi(x, y))| \bigtriangledown \varphi(x, y)| + \lambda \left(\sum_{U_i} |c_k - c_i| + \sum_{U_o} |c_k - c_o| \right) \cdot H_\varepsilon(\varphi(x, y)), \tag{11}$$

where $H_\varepsilon(z)$ and $\delta_\varepsilon(z)$ are the regularized forms of Heaviside function and Dirac function. The formulas for $H_\varepsilon(z)$ and $\delta_\varepsilon(z)$ are Equations (12) and (13), respectively:

$$H_\varepsilon(z) = \frac{1}{2}\left(1 + \frac{2}{\pi} arctan\left(\frac{z}{\varepsilon}\right)\right), \tag{12}$$

$$\delta_\varepsilon(z) = \frac{d}{dz} H_\varepsilon(z) = \frac{1}{\pi} \frac{\varepsilon}{\varepsilon^2 + z^2}. \tag{13}$$

Invoking the Euler-Lagrange equation to solve the energy functional, the following evolution Equation (14) can be obtained:

$$\frac{\partial \varphi}{\partial t} = \delta_\varepsilon(\varphi) \left[\mu \text{div}\left(\frac{\bigtriangledown \varphi}{| \bigtriangledown \varphi|}\right) + \lambda \left(\sum_{\mathrm{U_i}} |\mathrm{c_k} - \mathrm{c_i}| + \sum_{\mathrm{U_o}} |\mathrm{c_k} - \mathrm{c_o}| \right) \right], \tag{14}$$

where $\text{div}(\frac{\bigtriangledown \varphi}{|\bigtriangledown \varphi|})$ is the curvature of the level curve of φ.

$$\varphi(0, x, y) = \varphi_o(x, y) \text{ in } \Omega, \tag{15}$$

$$\frac{\delta_\varepsilon(\varphi)}{| \bigtriangledown \varphi|} \frac{\partial(\varphi)}{\partial \vec{n}} = 0 \text{ on } \partial\Omega, \tag{16}$$

where Equation (15) is the initial condition, and Equation (16) is the boundary condition. The mean value of perceived concentration is updated by the following formula during the iteration process:

$$\begin{aligned} c_i &= \frac{1}{N_i} \sum_{U_i} c_k \\ c_o &= \frac{1}{N_o} \sum_{U_o} c_k, \end{aligned} \tag{17}$$

where N_i is the number of sensor nodes inside the curve, and N_o is the number of sensor nodes outside the curve.

We differentiate nodes in the same USV by distance to the evolution curve and the string. If the distance from a node to the evolution curve is greater than its distance to the string, then we consider it inside the curve. Otherwise, it is outside the curve. Because the initial curve is a straight

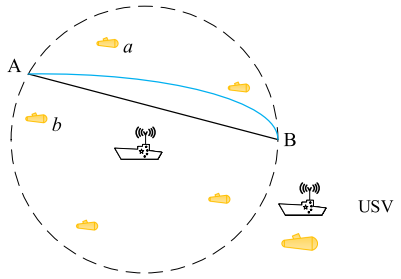

Fig. 2. Node location judgment.

line, it divides the nodes into two groups. According to these rules, it is stipulated that the top of the line is medial and the bottom is lateral.

As shown in Figure 2, the blue curve AB is the evolution curve calculated by the USV based on LSM. The dotted circle is the communication distance of the USV. A and B are the intersection points between the curve and the circle, with the USV at the center and the communication distance of the USV as the radius. The distance from node a to curve AB is less than the distance to chord AB, so node a is located outside the curve. Similarly, the distance from node b to curve AB is greater than the distance to chord AB, so node b is located inside the curve.

It is difficult to solve the partial differential equations in continuous form. Therefore, the level set equation needs to be discretized in a Cartesian grid with a spacing of h and a timestep of Δt and then solved using the finite difference method. At time n, the level set function of the point (i, j) is $\varphi(ih, ih, n\Delta t)$, and the level set equation can be discretized as Equation (8). Define the first-order difference operator matrix as:

$$E = \begin{bmatrix} \frac{\varphi_{i+1,j}-\varphi_{i-1,j}}{2h} & \frac{\varphi_{i,j+1}-\varphi_{i,j-1}}{2h} \\ \frac{\varphi_{i+1,j}-\varphi_{i,j}}{h} & \frac{\varphi_{i,j+1}-\varphi_{i,j}}{h} \\ \frac{\varphi_{i,j}-\varphi_{i-1,j}}{h} & \frac{\varphi_{i,j}-\varphi_{i,j-1}}{h} \end{bmatrix}. \tag{18}$$

In accordance with Equation (18), Equation (8) can be rewritten as:

$$\varphi_{ij}^{n+1} = \varphi_{ij}^{n} + \Delta t[max(v_{ij}^{n}, 0)\ \nabla^{+} + min(v_{ij}^{n}, 0)\ \nabla^{-} + \mu k_{ij}((e_{11})^2 + (e_{12})^2)^{1/2}], \tag{19}$$

where

$$\nabla^{+} = [max(e_{13}, 0)^2 + min(e_{12}, 0)^2 + max(e_{23}, 0)^2 + min(e_{22}, 0)^2]^{1/2}, \tag{20}$$

$$\nabla^{-} = [max(e_{12}, 0)^2 + min(e_{13}, 0)^2 + max(e_{22}, 0)^2 + min(e_{23}, 0)^2]^{1/2}, \tag{21}$$

$$v = \lambda \sum_{U_i} |c_k - c_i| + \lambda \sum_{U_o} |c_k - c_o|), \tag{22}$$

$$k_{ij} = \nabla \cdot \frac{\nabla \varphi}{|\nabla \varphi|} = \frac{\varphi_{xx}\varphi_y^2 - 2\varphi_x\varphi_y\varphi_{yy} + \varphi_{yy}\varphi_x^2}{(\varphi_x^2 + \varphi_y^2)^3/2}. \tag{23}$$

Nodes transmit the coordinate information and collected concentration information to the USV, which calculates the edge curve of the region of interest based on the information collected from the nodes. Algorithm 1 is the pseudocode for calculating the edge curve of the interest region based on LSM. The USV first establishes an initial curve based on its coordinate information and updates the corresponding $H_\varepsilon(z)$, $\delta_\varepsilon(z)$, and k_{ij} values based on the collected node concentration information and coordinate information (Steps 1~5). In Steps 6~16, the average concentration

ALGORITHM 1: Calculating Edge Curve of Interest Region

Require: initial curve $C : y = y_g$, USV communication range r^g, sensor communication range r^c, the maximal iteration number I, the number of nodes Q

Ensure: edge curve of the interest region $C : \varphi_{ij}^n = 0$

```
Establish the level set equation according to Equation (9) and establish the initialization curve C
for each n ∈ [1, I] do
    update H_ε(z) according to Equation (12)
    update δ_ε(z) according to Equation (13)
    update the curvature k_ij of the level set surface according to Equation (23)
    calculate the intersection points A and B of C and (x − x_g)^2 + (y − y_g)^2 = r^g2
    for each m ∈ [1, Q] do
        calculate the distance d_m^l from the node m to the line AB
        calculate the distance d_m^c from the node m to the curve AB
        if d_m^l > d_m^c then
            s_m ∈ U_o
        else
            s_m ∈ U_i
        end if
    end for
    c_i and c_o are updated using Equation (17)
    update the evolution curve C : φ_ij^n = 0 according to Equation (14)
end for
```

inside and outside the curve is updated by evaluating the position of the nodes with respect to the curve and the concentration of all nodes. Finally, the USV updates the edge curve C using Equation (14) and broadcasts the curve information to all nodes via the Broadcast_reply beacon. After receiving the edge curve information, the nodes adopt the movement strategy described in Section 4.1.2 to move. Algorithm 1 includes the nesting of two loop statements, from which the time complexity of the algorithm for calculating the edge curve of the interest region based on LSM can be derived as $O(mn)$, where m is the number of iterations and n is the number of nodes in the local calculation unit.

4.1.2 Node Mobility Strategy. The USV sends information regarding the edge curve and threshold value of the perceived concentration through BroadcastMG to all sensor nodes in the regional cell. The sensor nodes compare the perceived concentration value with the threshold value information. If the concentration value is greater than the threshold, then the nodes perceive that they are located in the region of interest. If the concentration value is lower than the threshold, then nodes perceive that they are outside the region of interest. The nodes move to new position coordinates based on the edge curve broadcasted by the USV. As the nodes get closer to the edge of the interest region, the changes in the received edge curve become smaller and the nodes move shorter distances. Eventually, the nodes continue monitoring their original positions and maintain fixed positions.

In theory, the sensor node will move along the vertical direction of the edge curve of the node and the interest region. However, due to the limitations of the computing algorithm and node computing power, it is difficult to find the point with the shortest distance from the node on the curve of the interest region. Therefore, considering the computing power and mobile energy

ALGORITHM 2: Node Movement Algorithm

Require: node position $\mathbf{p}_k = (x_k, y_k)$, the edge curve of interest region C
Ensure: new position $\mathbf{p}'_k$
1: calculate the intersection point $\mathbf{p}_x$ of C and $x = x_k$
2: calculate the intersection point $\mathbf{p}_y$ of C and $y = y_k$
3: calculate the distance d_x from $\mathbf{p}_k$ to $\mathbf{p}_x$
4: calculate the distance d_y from $\mathbf{p}_k$ to $\mathbf{p}_y$
5: **if** $d_x > d_y$ **then**
6: $\mathbf{p}_k = \mathbf{p}_y$
7: **else**
8: $\mathbf{p}_k = \mathbf{p}_x$
9: **end if**
10: $\mathbf{p}'_k = \mathbf{p}_k$

consumption of sensor nodes, the node will calculate its distance from the edge curve of the interest region and the coordinates of the intersection point in both horizontal and vertical directions and select the location with a short distance as the new position coordinates of the node. Algorithm 2 shows the pseudocode of node movement algorithm.

4.2 3D Underwater Space Sensor Node Deployment

Unlike 2D node deployment where the USV acts as a computing center, 3D underwater deployment adds the role of MEC-MSs. There are two reasons for adding MEC-MSs in 3D underwater deployment. First, unlike wireless communication on the surface, underwater acoustic speed is slow. If the sensor node communicates with the USV on the water surface, then it cannot guarantee timely network control. Direct communication between the sensor node and the MEC-MS is advantageous for reducing network latency. Second, lightweight edge-computing stations are deployed on the MEC-MS equipment, which can effectively relieve the computing pressure on the USV.

We assume that USVs are uniformly distributed on the water surface, sensor nodes are randomly scattered in the underwater space, and the size of the target monitoring water area is $L \times W \times H$. The sensor nodes and MEC-MS can move freely, and there is a certain distance between the MEC-MS and sensor nodes. In the working process of an underwater sensor network, sensor nodes use acoustic communication to transmit collected information to the MEC-MS via single-hop or multi-hop paths, and the MEC-MS performs unified scheduling of the sensor nodes in its search domain. MEC-MSs in different domains then transmit the information to USVs, which then transmit the information to the data center for analysis via satellite or ground stations. Figure 3 shows the architecture diagram of a typical underwater wireless sensor network.

All sensor nodes send and receive signals uniformly in all directions. The sensing range of the sensor node is a spherical area with the node as the center and a radius of r. The following assumptions are established:

- All sensor nodes in the network, except for the MEC-MS, have the same communication distance, and the communication distance of the MEC-MS is greater than that of the sensor nodes.
- Sensor nodes can perceive their location and the location of their neighbors and can obtain information about the current water concentration.

Assume that all mobile nodes are randomly distributed in the 3D underwater space in advance and the distance between all nodes and neighboring nodes is within the node communication

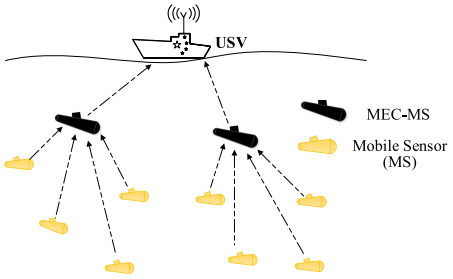

Fig. 3. 3D underwater architecture model.

ALGORITHM 3: 3D Underwater Node Deployment Algorithm

Require: mobile nodes position $\mathbf{p}_k$, concentration value c_k
Ensure: new position $\mathbf{p}'_k$

1: MEC-MS calculates the depth interval $depth[i, j] \in H$ of the concentration change according to the concentration value c_k and coordinate value $\mathbf{p}_k$ transmitted by the mobile sensor node.
2: Calculate the intersection point $\mathbf{p}_y$ of C and $y = y_k$. All sensor nodes outside the z-coordinate interval $depth[i, j]$ move vertically to the z-coordinate $\frac{i+j}{2}$ and transmit the position information and the concentration value of the new position again.
3: According to Algorithm 1, the edge curve calculation of all node information at the z-axis coordinate $\frac{i+j}{2}$ is carried out to obtain the edge curve C of the interest area.
4: All nodes keep the axis coordinates unchanged, calculate the new coordinate position $\mathbf{p}'_k$, and move horizontally to the new position according to Algorithm 2.

range. That is, the information of all nodes can be transmitted to the MEC-MS through single-hop or multihop paths, and the MEC-MS can also transmit information to mobile sensor nodes. The communication protocols of Section 3.2 are still applicable to 3D underwater space systems. Based on the 2D plane sensor node deployment scheme in the previous section, we extend it to 3D underwater space. The sensor node deployment scheme is shown in Algorithm 3.

Compared with the 2D deployment method, the communication framework of the 3D deployment method has two differences. First, in terms of localization, the nodes request localization from the MEC-MS via Report_request, and the MEC-MS then requests localization from the USV. The USV responds to the MEC-MS with the localization results through Report_reply, and the MEC-MS then replies to the nodes with the localization results. Second, the MEC-MS replaces the USV as the computing center, and the nodes communicate with the MEC-MS using BroadcastMG beacons. The nodes request edge curve information from the MEC-MS through Broadcast_request, and the MEC-MS calculates the edge curve based on node coordinates and concentration information. Then, the MEC-MS uses Broadcast_reply to broadcast the computed edge curve to all nodes.

4.3 Performance Evaluation Metrics

The main goal of existing research on underwater sensor node deployment is to use as few nodes as possible to cover the underwater area or point events, whereas the goal of our hunting-style node deployment aims to cover and track the boundary of the interest region. Inspired by the evaluation metrics of edge detection in image processing, the following performance evaluation metrics are established:

4.3.1 Structural Similarity. **Structural Similarity (SSIM)** is an index that measures the similarity of two images and is commonly used in the performance evaluation of image edge detection [26, 33, 47]. Therefore, it is highly suitable for the evaluation of the quality of the level set-based sensor node arrangement method proposed in this article. The SSIM evaluation system defined in this article consists of both structural length and concentration comparisons. The structure length comparison function is:

$$p(a,b) = \frac{min\{p_a, p_b\}}{max\{p_a, p_b\}}, \tag{24}$$

where a is the edge of the interest region, and b is the edge connected by the sensor node. p_a is the edge length of the interest region, and p_b is the edge length of the sensor node connection. The concentration contrast function is:

$$c(a,b) = \frac{\sigma_{ab} + m}{\sigma_a \sigma_b + m}, \tag{25}$$

where

$$\sigma_a = \left(\frac{1}{N-1} \sum_{i=1}^{N} (a_i - c_a)^2 \right)^{1/2}, \tag{26}$$

$$\sigma_b = \left(\frac{1}{N-1} \sum_{i=1}^{N} (b_i - c_b)^2 \right)^{1/2}, \tag{27}$$

$$\sigma_{ab} = \frac{1}{N-1} \sum_{i=1}^{N} (a_i - c_a)(b_i - c_b)). \tag{28}$$

The structural similarity metric is obtained through the synthesis of these two functions:

$$SSIM(a,b) = [p(a,b)]^{\alpha} [c(a,b)]^{\beta}, \tag{29}$$

where α and β are used to adjust the relationship between the two modules. The larger the value of SSIM, the closer the node is to the edge of the interest region.

4.3.2 Network Energy Balance. Whether the energy consumption is uniform to the nodes in the UWSN is directly related to the survival time of the network, so in this research, it is necessary to evaluate the energy consumption balance of each sensor node in terms of data transmission. Let the energy consumption of the node s_k be E_{sk} and the mean square error $\sigma(E)$ of the energy consumption of all nodes as the node energy balance. It can be seen that the smaller $\sigma(E)$, the more balanced the network energy consumption and technical feasibility.

The energy consumption of underwater sensor nodes mainly includes mobile energy consumption and acoustic communication energy consumption. When the node arrangement encounters a relatively steady state, its main energy consumption is acoustic communication energy consumption. The acoustic channel model [8] considered here is mainly characterized by signal attenuation and noise in the environment. It depends on the distance l of signal transmission and its frequency f. We calculate the energy consumption of k (bit) data transmitting distance l (m) at the node using the loss model of underwater acoustic signal propagation:

$$E_{Tx} = k \cdot T_p \cdot P_0 \cdot A(l,f), \tag{30}$$

where T_p is the unit data transmission time. P_0 is the lowest power that the receiving end can normally receive the signal, and its unit is watt. The signal attenuation is given by Equation (31), where A_0 is a unit normalization constant, k is the spreading factor, $a(f)$ is the absorption coefficient, and f (kHz) is in dB/km.

$$10 \log A(l,f)/A_0 = 10k \log l + 10l \log \alpha(f) \tag{31}$$

Table 1. Parameter Settings

Parameter name	Value
Monitoring area (m)	300 × 300
Number of USV	4
The communication radius of the USV (m)	100
Number of sensor nodes	40/60
The communication radius of the sensor node (m)	50
Initial energy consumption of sensor node (J)	1,000
Information transmission power (W)	0.05
Mobile energy consumption of sensor node (J/m)	0.5
Dirac function constant ε	1
Acoustic velocity	1,500 m/s
Simulation period	3,000 timeslots

The first term of Equation (31) represents the propagation loss, whereas the second term represents the absorption loss. The spreading factor k describes the geometry of the propagation, with common values of 1 (cylindrical spreading), 1.5 (practical spreading), and 2 (spherical spreading). The absorption coefficient $a(f)$ is expressed by Thorpe's formula.

$$10\log\alpha(f) = 0.11\frac{f^2}{1+f^2} + 44\frac{f^2}{4,100+f^2} + 2.75\cdot 10^{-4}f^2 + 0.003 \tag{32}$$

Let the power of a node move per unit distance be M_p (W). Therefore, the energy consumption of the node moving distance l (m) can be calculated by:

$$E_{Mx} = M_p \cdot l. \tag{33}$$

The total energy consumption of the node is the sum of these two energy consumptions:

$$E_{sx} = E_{Tx} + E_{Mx}. \tag{34}$$

Therefore, the network energy balance can be calculated by:

$$\sigma(E) = \sqrt{\frac{1}{N}\sum_{i=1}^{n}(E_{sk} - \mu_E)}, \tag{35}$$

where μ_E is the average energy consumption of all nodes.

5 PERFORMANCE ANALYSIS AND SIMULATION

5.1 Simulation Setup

This section evaluates the effectiveness of the underwater sensor node deployment method based on LSM. Simulation experiments were carried out on the MATLAB R2018b platform, and the computer configurations are given as follows: 2.90 GHz CPU and 8.0 GB RAM. The network is deployed in a 2D water area of 300 m × 300 m. The four USVs are evenly distributed on the target water surface. The horizontal and vertical distances between adjacent USVs are both 150 m. Sensor nodes are randomly deployed on the water surface. There are no errors in the boundary of the interest region and the positioning accuracy of sensor nodes. The parameter settings used in the simulation are shown in Table 1.

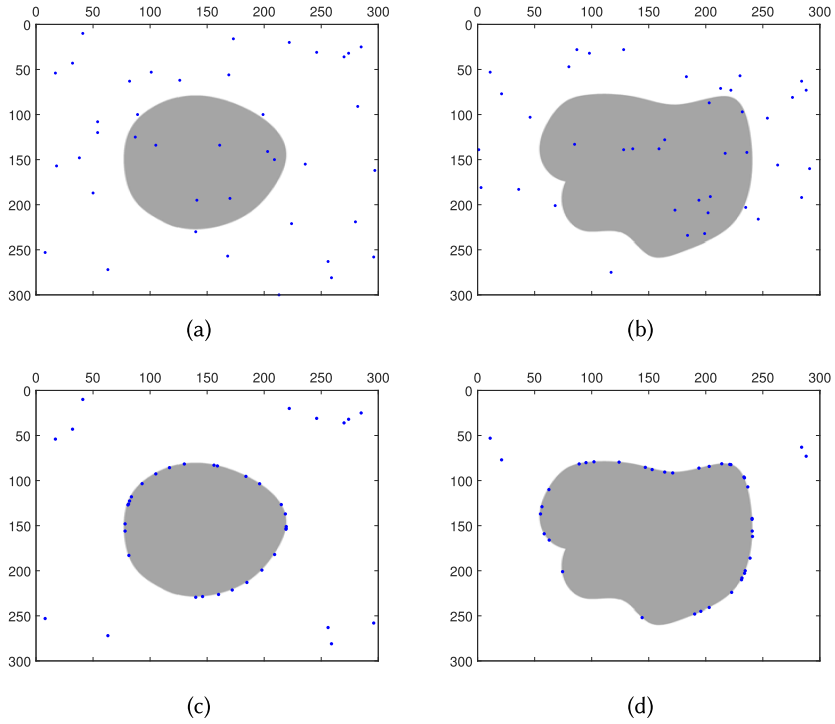

Fig. 4. 2D sensors hunt interest regions with 40 sensors. (a) Initial network deployment for elliptical region of interest. (b) Initial network deployment for irregular shape region of interest. (c) Nodes hunt ellipse region of interest. (d) Nodes hunt irregular shape region of interest.

5.2 Results and Analysis

5.2.1 Availability of the SD-LSM. Based on these parameters, six sets of plane verification experiments and two sets of 3D scene realizations were designed in the monitoring area. Experiment 1: Irregular shape interest region with four USVs and 40 sensors. Experiment 2: Elliptical interest region with four USVs and 40 sensors. Experiment 3: Irregular shape interest region with four USVs and 60 sensors. Experiment 4: Elliptical interest region with four USVs and 60 sensors. Experiment 5: 3D single irregular shape interest region with four MEC-MSs and 100 sensor nodes. Experiment 6: 3D multiple irregular shape interest region with four MEC-MSs and 100 sensor nodes. In the experiment, the interest region is spread out evenly.

Figures 4 and 7 show the experimental results of the six groups of experiments. In these figures, a dot indicates a sensor node, and the gray area represents the interest region. Take Figures 5(b) and 6(a) as examples; the number of sensor nodes is 60 and 100, respectively. The experimental simulations are performed on the 2D irregular interest region and the 3D irregular interest region, respectively. The experimental results are shown in Figures 5(d) and 7(a), respectively. It can be seen that the algorithm of this article can realize the autonomous trend of nodes and deploy on the edge of the interest region. The more sensor nodes perceive the boundary of the interest region, the better the hunting effect at the edge of the interest region.

5.2.2 Structural Similarity. Existing deployment algorithms use event point-driven underwater sensor node deployment methods, and the algorithm proposed in this article is a region-of-interest-driven deployment method to achieve the purpose of hunting the region of interest. Because all

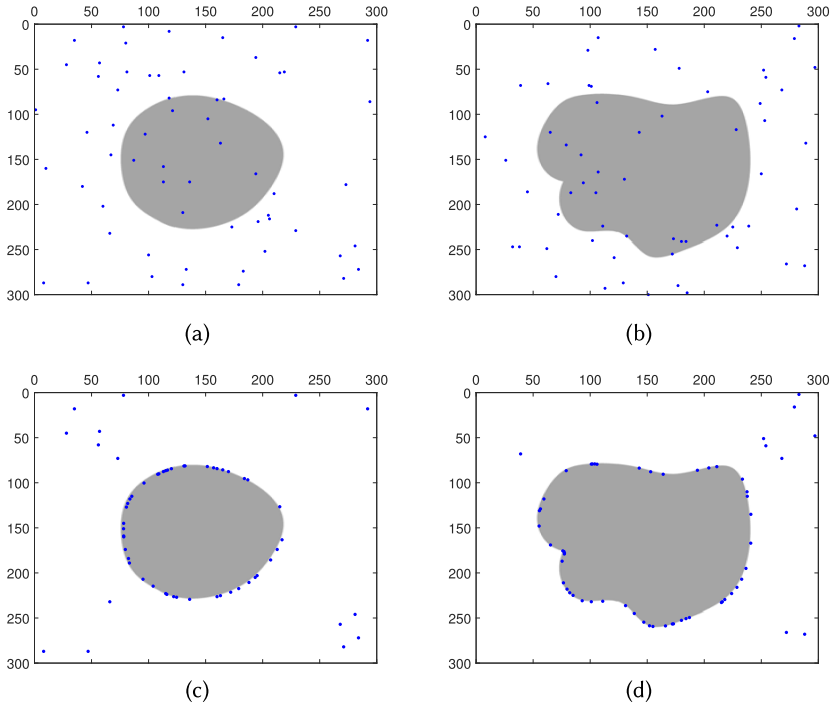

Fig. 5. 2D sensors hunt interest regions with 60 sensors. (a) Initial network deployment for elliptical region of interest. (b) Initial network deployment for irregular shape region of interest. (c) Nodes hunt ellipse region of interest. (d) Nodes hunt irregular shape region of interest.

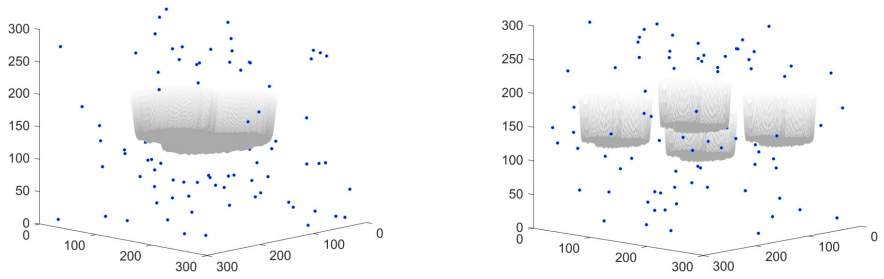

(a) Single irregular shape interest region (b) Multiple irregular shape interest regions

Fig. 6. 3D irregular shape interest regions with 100 sensors.

tasks are completed with the assistance of multiple mobile nodes, we compare SD-LSM with the method proposed in Reference [23]. We also compare the basic method of random movement, in which each node moves randomly and stops moving if the pollution concentration is currently sensed at the location and no pollution concentration is present at its next location. The performance of the algorithm is evaluated using the two indicators of structural similarity and network energy balance proposed in Section 4.2. Twenty repeated experiments are carried out for each prior experiment to assess the two evaluation metrics of structural similarity and average energy consumption.

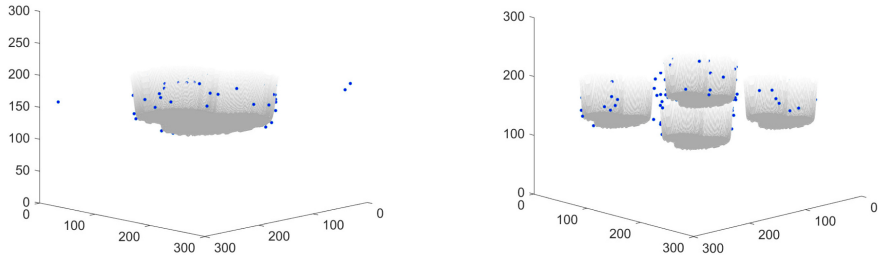

(a) Single irregular shape interest region (b) Multiple irregular shape interest regions

Fig. 7. 3D sensors hunt interest region with 100 sensors.

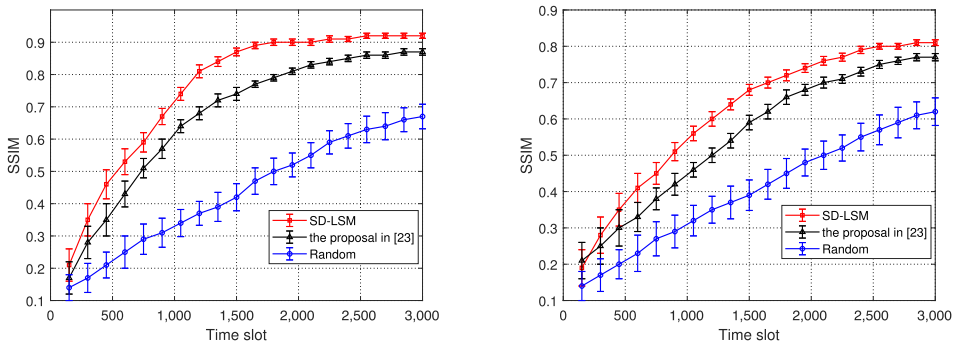

(a) Elliptical interest region (b) Irregular shape interest region

Fig. 8. SSIM evolution process comparison with different schemes.

Figure 8 presents the statistical results of structural similarity for the different methods. The number of nodes is 60, the timeslot is 0.1 s, and the results are refreshed every 150 timeslots. Figure 8(a) shows statistics for an elliptical region of interest. The SSIM of SD-LSM increases with the increase in timeslots. At around 1,500 timeslots, the SSIM value reaches a plateau of approximately 0.9. The black curve represents the structural similarity of the proposed method in Reference [23] when the timeslot is varied. The SSIM of this method increases with the increase in timeslots. At around 2,000 timeslots, the SSIM value tends to stabilize, reaching approximately 0.83. To prevent the random method from having a large step size that leads to poor trapping performance, we set the step size of the random method to gradually decrease over time. The SSIM of the random method increases with the increase in timeslots, reaching a maximum value of 0.67. As expected, SD-LSM achieves a higher SSIM compared to the method proposed in Reference [23] and the random method, and it reaches the edges of the region of interest faster. Figure 8(b) shows statistics for an irregular region of interest, indicating that the SSIM values for the elliptical region are higher than those for the irregular region.

5.2.3 Average Energy Consumption. Figure 9 shows the average energy consumption for these methods. In Figure 9(a), the average energy consumption of SD-LSM increases gradually with increasing timeslots. Between 150 and 1,500 timeslots, the energy consumption of SD-LSM is close to that of the other two methods, because the main energy consumption is mobile energy consumption. After 1,500 timeslots, the energy consumption of SD-LSM increases slowly, because the movement of the nodes decreases rapidly after reaching the edge of the region of interest and the main energy consumption relates to beacon transmission. The method proposed in Reference [23]

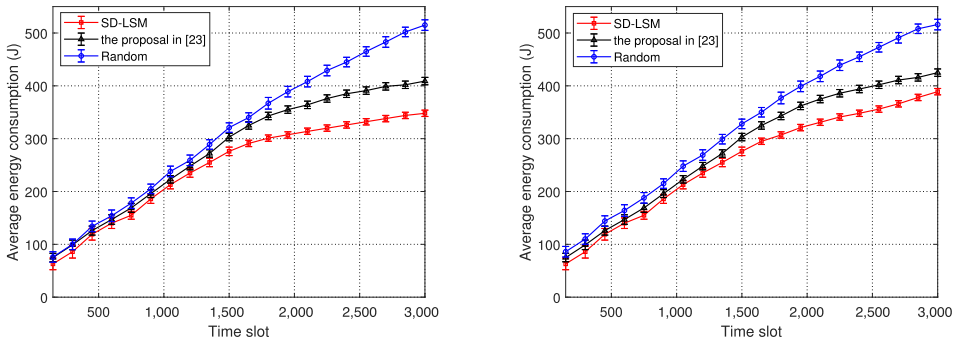

(a) Elliptical interest region (b) Irregular shape interest region

Fig. 9. Average energy consumption of sensor nodes comparison with different schemes.

shows a slowdown in energy consumption growth after 2,000 slots. When AUVs reach a specific point on the boundary of the region of interest, they need to move along the contour of the boundary, so the energy consumption is higher compared with SD-LSM. The energy consumption of the random method increases with the increase in timeslots, and movement causes a large amount of mobile energy consumption, much higher than the two other schemes. Figure 9(b) shows the statistical results for an irregular region of interest, which consumes slightly more energy than an elliptical region of interest.

5.2.4 Average Control Delay. To evaluate the time required for executing real-time underwater control, we test the average delay of nodes requesting control messages from the MEC-MS at different timeslots, and the results are shown in Figure 10. The delay is influenced by the distance between each node and the MEC-MS. Figures 10(a) and 10(b) show simulations for elliptical and irregular regions of interest, respectively, and the delay trends are approximately the same for both. The delay of SD-LSM decreases as the timeslots increase, then levels off. This is due to the initial random distribution of nodes being farther from the MEC-MS, and as the nodes move toward the region of interest, they are more concentrated and the average control delay decreases. The method proposed in Reference [23] requires moving along contour lines when reaching certain boundaries, which slightly increases the control delay. The random method does not have a centralized computing center and, thus, there is no control delay. Although the control delay of SD-LSM is slightly higher than the method proposed in Reference [23], the overall average delay is within 1.4 seconds.

5.2.5 Performance Comparison with Different Node Quantities. We select different numbers of sensor nodes and different shapes of interest regions for analysis with 1,500 timeslots. The detailed statistical results for the average structural similarity, network energy balance, and control latency achieved through the SD-LSM and the method proposed in Reference [23] can be found in Table 2. The results show how as the number of sensors increases, the SSIM value also increases. For the same number of sensor nodes, the SSIM for an elliptical interest region is larger than that of an irregular interest region, and as the number of sensors increases, the network energy balance increases.

6 CONCLUSION

This research proposes a method of hunting deployment of underwater sensors based on LSM. In this method, a gateway-like role organizes the sensor nodes in its communication range to form local computing units according to the concentration information sensed by the sensor nodes

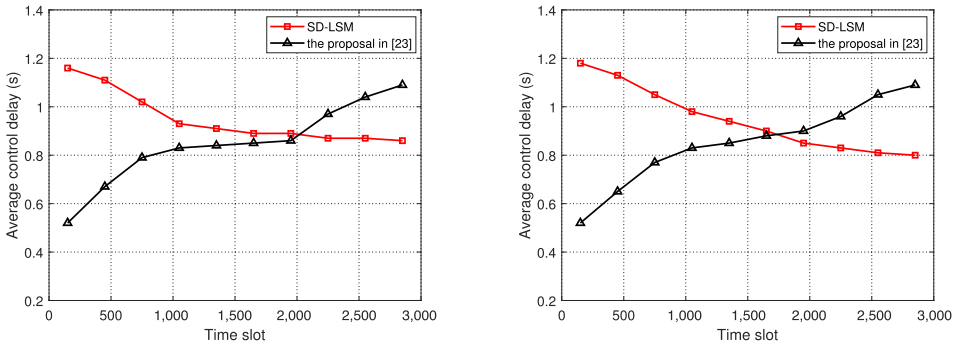

(a) Elliptical interest region (b) Irregular shape interest region

Fig. 10. Test for average control delay.

Table 2. Statistics of Experimental Results

Number of sensors	Region of interest shape	SD-LSM			the proposal in [23]		
		SSIM	σ_E	delays	SSIM	σ_E	delays
40	Irregular shape	0.6082	0.3862	0.73	0.5586	0.4148	0.69
	Elliptical	0.7453	0.3984	0.72	0.6547	0.4294	0.70
50	Irregular shape	0.6328	0.4591	0.75	0.5742	0.5023	0.68
	Elliptical	0.8096	0.4711	0.79	0.7138	0.4814	0.71
60	Irregular shape	0.6734	0.5402	0.91	0.6054	0.5835	0.86
	Elliptical	0.8702	0.5586	0.90	0.7478	0.6041	0.85
70	Irregular shape	0.7854	0.5762	1.01	0.6512	0.5649	0.89
	Elliptical	0.8936	0.5735	0.96	0.7825	0.5813	0.88
80	Irregular shape	0.8138	0.5894	1.17	0.7932	0.6218	1.12
	Elliptical	0.9256	0.5986	1.21	0.8675	0.6231	1.08

and subsequently constructs a calculation model driven by energy function. The nodes in the computing unit simulate the LSM dynamic evolution mechanism to obtain the edge information of the interest region. Each sensor node calculates its dynamic parameters, combining its position and edge information, and migrates toward the edge of the interest region autonomously. The migration of a large number of nodes can gradually evolve into hunting deployment on the edge of the interest region to realize coverage and monitoring. Two performance evaluation metrics—structural similarity and network energy balance—are used to evaluate the comprehensive performance of the proposed method. A large number of simulation experiments show that this method can achieve dynamic and hunting coverage of the edge of the interest region with different node numbers and interest region shapes, consequently achieving effective tracking and monitoring of the interest region.

As a future work, we intend to test self-developed USVs in an actual underwater environment and verify the effectiveness of nodes in tracking water pollution.

REFERENCES

[1] Faiza Al-Salti, Khaled Day, Nasser Alzeidi, and Abderezak Touzene. 2018. Multiple sink placement strategy for underwater wireless sensor networks. In *International Symposium on Networks, Computers and Communications (ISNCC)*. 1–6.

[2] D. Arivudainambi, Sethuraman Balaji, and T. S. Poorani. 2017. Sensor deployment for target coverage in underwater wireless sensor network. In *International Conference on Performance Evaluation and Modeling in Wired and Wireless Networks (PEMWN)*. 1–6.

[3] Tong Bai, Cunhua Pan, Yansha Deng, Maged Elkashlan, Arumugam Nallanathan, and Lajos Hanzo Hanzo. 2020. Latency minimization for intelligent reflecting surface aided mobile edge computing. *IEEE J. Select. Areas Commun.* 38, 11 (2020), 2666–2682.

[4] Thanh Minh Bui, Alain Coron, Jonathan Mamou, Emi Saegusa-Beecroft, Tadashi Yamaguchi, Eugene Yanagihara, Junji Machi, S. Lori Bridal, and Ernest J. Feleppa. 2017. Local transverse-slice-based level-set method for segmentation of 3-D high-frequency ultrasonic backscatter From dissected human lymph nodes. *IEEE Transactions on Biomedical Engineering* 64 (2017), 1579–1591.

[5] Scott G. Burman, Jingya Gao, Gregory B. Pasternack, Nann A. Fangue, Paul Cadrett, Elizabeth Campbell, and Dipak Ghosal. 2022. TempMesh—A flexible wireless sensor network for monitoring river temperatures. *ACM Trans. Sensor Netw.* 19 (2022), 1–28.

[6] Tony F. Chan and Luminita A. Vese. 1999. An active contour model without edges. In *Scale-Space Theories in Computer Vision*. Springer, Berlin Heidelberg, 141–151. https://doi.org/10.1007/3-540-48236-9_13

[7] Rodolfo W. L. Coutinho and Azzedine F. M. Boukerche. 2021. OMUS: Efficient opportunistic routing in multi-modal underwater sensor networks. *IEEE Trans. Wirel. Commun.* 20 (2021), 5642–5655.

[8] Zhengru Fang, Jingjing Wang, Chunxiao Jiang, Biling Zhang, Chuan Qin, and Yong Ren. 2020. QLACO: Q-learning aided ant colony routing protocol for underwater acoustic sensor networks. In *IEEE Wireless Communications and Networking Conference (WCNC)*. 1–6.

[9] Hengqing Ge, Guibin Chen, and Guang Xu. 2018. Multi-AUV cooperative target hunting based on improved potential field in a surface-water environment. *Appl. Sci.* 8, 6 (2018), 973.

[10] Sanghai Guan, Jingjing Wang, Chunxiao Jiang, Ruiyang Duan, Yong Ren, and Tony Q. S. Quek. 2021. MagicNet: The maritime giant cellular network. *IEEE Commun. Mag.* 59 (2021), 117–123.

[11] Hui Guo, Zhaoyong Mao, Wenjun Ding, and Peiliang Liu. 2019. Optimal search path planning for unmanned surface vehicle based on an improved genetic algorithm. *Comput. Electric. Eng.* 79 (2019), 106467.

[12] Song Han, Zhang Tao, Xinbin Li, Junzhi Yu, Tongwei Zhang, and Zhixin Liu. 2022. The unified task assignment for underwater data collection with multi-AUV system: A reinforced self-organizing mapping approach. *IEEE Trans. Neural Netw. Learn. Syst.* (2022), 1–14. https://doi.org/10.1109/TNNLS.2022.3185611

[13] Xiangwang Hou, Jingjing Wang, Tong Bai, Yansha Deng, Yong Ren, and Lajos Hanzo Hanzo. 2022. Environment-aware AUV trajectory design and resource management for multi-tier underwater computing. *IEEE J. Select. Areas Commun.* 41 (2022), 474–490.

[14] Kun Hu, Shuyou Zhang, and Xinyue Zhao. 2018. An energy-minimizing level set method for defect detection. *Wirel. Person. Commun.* 102 (2018), 3545–3555.

[15] Imad Jawhar, Nader Mohamed, Jameela Al-Jaroodi, and Shengyou Zhang. 2019. An architecture for using autonomous underwater vehicles in wireless sensor networks for underwater pipeline monitoring. *IEEE Trans. Industr. Inform.* 15 (2019), 1329–1340.

[16] Peng Jiang, Yang Feng, and Feng-Nien Wu. 2016. Underwater sensor network redeployment algorithm based on wolf search. *Sensors (Basel)* 16 (2016).

[17] Zhigang Jin, Zhihua Ji, Yishan Su, Shuo Li, and Boyao Wei. 2018. A deployment optimization mechanism using depth adjustable nodes in underwater acoustic sensor networks. In *MTS/IEEE Kobe Techno-Oceans Conference (OTO)*. 1–6.

[18] Berkay Kahriman, Ali Murat Demirtas, and Bulent Tavli. 2020. Surface gateway placement optimization for underwater sensor networks. In *28th Telecommunications Forum (TELFOR)*. 1–4.

[19] Sunhyo Kim and Jee Woong Choi. 2017. Optimal deployment of sensor nodes based on performance surface of underwater acoustic communication. *Sensors (Basel)* 17 (2017).

[20] S. Vinoth Kumar, Raman Jayaparvathy, and B. N. Priyanka. 2020. Efficient path planning of AUVs for container ship oil spill detection in coastal areas. *Ocean Eng.* 217 (2020), 107932.

[21] Qihao Li, Ning Zhang, Michael Cheffena, and Xuemin (Sherman) Shen. 2020. Channel-based optimal back-off delay control in delay-constrained industrial WSNs. *IEEE Trans. Wirel. Commun.* 19 (2020), 696–711.

[22] Francisco H. M. B. Lima, Luiz Filipe M. Vieira, Marcos Augusto M. Vieira, Alex Borges Vieira, and José Augusto Miranda Nacif. 2019. Water ping: ICMP for the internet of underwater things. *Comput. Netw.* 152 (2019), 54–63.

[23] Chuan Lin, Guangjie Han, Jiaxin Du, Yuanguo Bi, Lei Shu, and Kaiguo Fan. 2020. A path planning scheme for AUV flock-based internet-of-underwater-things systems to enable transparent and smart ocean. *IEEE Internet Things J.* 7 (2020), 9760–9772. DOI: https://doi.org/10.1109/JIOT.2020.2988285

[24] Lingfeng Liu, Chunfeng Liu, Yantai Shu, and Maode Ma. 2018. Optimal relay node placement for connectivity recovery in underwater acoustic sensor networks. In *IEEE International Conference on Information Communication and Signal Processing (ICICSP)*. 33–37.

[25] Lingfeng Liu, Maode Ma, Chunfeng Liu, and Yantai Shu. 2017. Optimal relay node placement and flow allocation in underwater acoustic sensor networks. *IEEE Trans. Commun.* 65 (2017), 2141–2152.
[26] Kede Ma, Zhengfang Duanmu, Hojatollah Yeganeh, and Zhou Wang. 2018. Multi-exposure image fusion by optimizing a structural similarity index. *IEEE Trans. Computat. Imag.* 4 (2018), 60–72.
[27] K. P. Nariratih and Dian Nur Rahmawati. 2019. Smart Kampung: Characterisation of Surabaya urban coastal settlements through smart city measurement. *IOP Conf. Series: Earth Environ. Sci.* 396 (2019).
[28] Stanley J. Osher and James A. Sethian. 1988. Fronts propagating with curvature-dependent speed: Algorithms based on Hamilton-Jacobi formulations. *Journal of Computational Physics* 79, 1 (1988), 12–49.
[29] Xingyue Qi, Chuan Lin, Zhaohui Wang, Jiaxin Du, and Guangjie Han. 2021. Proactive alarming-enabled path planning for multi-AUV-based underwater IoT systems. In *Computing, Communications and IoT Applications Conference (ComComAp)*. 263–267. DOI: https://doi.org/10.1109/ComComAp53641.2021.9652962
[30] Robert L. Runkel and Kenneth E. Bencala. 1995. *Transport of Reacting Solutes in Rivers and Streams*. Springer Netherlands, 137–164. https://doi.org/10.1007/978-94-017-1439-6_5
[31] Nasir Saeed, Tareq Y. Al-Naffouri, and Mohamed-Slim Alouini. 2019. Outlier detection and optimal anchor placement for 3-D underwater optical wireless sensor network localization. *IEEE Trans. Commun.* 67 (2019), 611–622.
[32] Dr. Sandeep and Vinay Kumar. 2017. Review on clustering, coverage and connectivity in underwater wireless sensor networks: A communication techniques perspective. *IEEE Access* 5 (2017), 11176–11199.
[33] Yalda Shahriari, Richard L. Fidler, Michele M. Pelter, Yong Bai, Andrea Villaroman, and Xiao Hu. 2018. Electrocardiogram signal quality assessment based on structural image similarity metric. *IEEE Trans. Biomed. Eng.* 65 (2018), 745–753.
[34] Lei Su, Ji Fan, and Linhan Fu. 2020. Exploration of smart city construction under new urbanization: A case study of Jinzhou-Huludao coastal area. *Sustain. Comput. Inform. Syst.* 27 (2020), 100403.
[35] Yishan Su, Lei Guo, Zhigang Jin, and Xiaomei Fu. 2020. A Voronoi-based optimized depth adjustment deployment scheme for underwater acoustic sensor networks. *IEEE Sensors J.* 20 (2020), 13849–13860.
[36] Peng Sun and Azzedine F. M. Boukerche. 2018. Modeling and analysis of coverage degree and target detection for autonomous underwater vehicle-based system. *IEEE Trans. Vehic. Technol.* 67 (2018), 9959–9971.
[37] Minjie Wan, Guohua Gu, Jianhong Sun, Weixian Qian, Kan Ren, Qian Chen, and Xavier P. V. Maldague. 2018. A level set method for infrared image segmentation using global and local information. *Remote. Sens.* 10 (2018), 1039.
[38] Chengcai Wang, Jun Lu, Xilun Ding, Chunxiao Jiang, Jianying Yang, and Jianhua Shen. 2021. Design, modeling, control, and experiments for a fish-robot-based IoT platform to enable smart ocean. *IEEE Internet Things J.* 8 (2021), 9317–9329.
[39] Sai Wang, Thu L. N. Nguyen, and Yoan Shin. 2018. Data collection strategy for magnetic induction based monitoring in underwater sensor networks. *IEEE Access* 6 (2018), 43644–43653.
[40] Tian Wang, Dan Zhao, Shaobin Cai, Weijia Jia, and Anfeng Liu. 2020. Bidirectional prediction-based underwater data collection protocol for end-edge-cloud orchestrated system. *IEEE Trans. Industr. Inform.* 16 (2020), 4791–4799.
[41] Zhongsi Wang and Bang Wang. 2017. A novel node sinking algorithm for 3D coverage and connectivity in underwater sensor networks. *Ad Hoc Netw.* 56 (2017), 43–55.
[42] Na Xia, Yin Wang, Bin Chen, Huazheng Du, Chaonong Xu, and Rong Zheng. 2023. IMF2O2: A fully connected sensor deployment algorithm for underwater sensor networks. *ACM Trans. Sensor Netw.* 19, 3 (2023), 1–22.
[43] Jing Yan, Ziqiang Xu, Xiaoyuan Luo, Cailian Chen, and Xinping Guan. 2019. Feedback-based target localization in underwater sensor networks: A multisensor fusion approach. *IEEE Trans. Sig. Inf. Process. Netw.* 5 (2019), 168–180.
[44] Jing Yan, Xian Yang, Xiaoyuan Luo, and Cailian Chen. 2018. Energy-efficient data collection over AUV-assisted underwater acoustic sensor network. *IEEE Syst. J.* 12 (2018), 3519–3530.
[45] Zhaoquan Zeng, Shu Fu, Huihui Zhang, Yuhan Dong, and Julian Cheng. 2017. A survey of underwater optical wireless communications. *IEEE Commun. Surv. Tutor.* 19 (2017), 204–238.
[46] Hao Zhang, Shi-Lian Wang, and Haixin Sun. 2016. Research on water surface gateway deployment in underwater acoustic sensor networks. In *MTS/IEEE Monterey Conference*. 1–7.
[47] Lei Zhang, Fengbao Yang, and Linna Ji. 2017. Multi-scale fusion algorithm based on structure similarity index constraint for infrared polarization and intensity images. *IEEE Access* 5 (2017), 24646–24655.
[48] Ying Zhang, Zheming Zhang, Lei Chen, and Xinheng Wang. 2021. Reinforcement learning-based opportunistic routing protocol for underwater acoustic sensor networks. *IEEE Trans. Vehic. Technol.* 70 (2021), 2756–2770.
[49] Daqi Zhu, Bei Zhou, and Simon X. Yang. 2021. A novel algorithm of multi-AUVs task assignment and path planning based on biologically inspired neural network map. *IEEE Trans. Intell. Vehic.* 6 (2021), 333–342.
[50] Muhammed Çobanlar, Huseyin Ugur Yildiz, Vahid Khalilpour Akram, Orhan Dagdeviren, and Bulent Tavli. 2022. On the tradeoff between network lifetime and k-connectivity-based reliability in UWSNs. *IEEE Internet Things J.* 9 (2022), 24444–24452.

Received 6 February 2023; revised 21 May 2023; accepted 5 June 2023